Supplementary information for:

Permeability transition in human mitochondria persists in the absence of peripheral stalk subunits of ATP synthase

Jiuya He, Joe Carroll, Shujing Ding, Ian M. Fearnley and John E. Walker

Medical Research Council Mitochondrial Biology Unit, University of Cambridge, Cambridge Biomedical Campus, Hills Road, Cambridge CB2 0XY, United Kingdom

General Methods. *ATP5F1* and *ATP5O* were disrupted in HAP1-WT cells by CRISPR-Cas9 technology (1), employing the gRNAs listed in Table S1. The HAP1-WT and clonal cells, HAP1-Δb and HAP1-ΔOSCP, were grown under standard conditions, and their growth rates were determined with an IncuCyte HD instrument. Mitoplasts were prepared from cells as described before (2, 3). Extracts of mitoplasts, made with 1% (w:v) DDM, were fractionated by SDS-PAGE, and subunits b and OSCP and citrate synthase were detected by western blotting. The oligomeric states of ATP synthase and vestigial complexes, and complexes I, II, III and IV, were examined by analysis of DDM and digitonin extracts of mitoplasts by BN-PAGE and western blotting. The ATP synthase complexes were detected with antibodies against the β-, g-, d-and F_6-subunits, and complexes I, II, III and IV with antibodies against NDUFS2, SDHA, UQCRC1, and COX4, respectively. The origins of the antibodies are given in Table S6. The oxygen consumption rates of HAP1-WT, HAP1-Δb and HAP1-ΔOSCP cells were measured in a Seahorse XFe24 instrument (3). ATP synthase was purified from mitoplasts by immuno-capture (3), and analysed by SDS-PAGE. Proteins in Coomassie blue stained bands were digested with trypsin (4) and peptides were identified by sequencing by mass spectrometry. Stable isotope labelling of proteins with amino acids in cell culture (5) (SILAC) of HAP1-WT, HAP1-Δb and HAP1-ΔOSCP cells was carried out as described before (3). After

labelling, the proteins in mitoplast samples or immuno-purified ATP synthase preparations were fractionated by SDS-PAGE, and quantitated by mass spectrometry (6). Protein ratios for the various forms of IF_1 were calculated as before (3). The protein ratios for subunit b in the samples of ATP synthase immuno-purified from SILAC labelled control and HAP1-Δb cells were re-calculated manually (median of peptide ratios) from the MaxQuant evidence file, after excluding peptide ratios assigned to a truncated form of the protein expressed in HAP1-Δb cells (see Results). The protein ratio for the OSCP in the sample of ATP synthase immuno-purified from control light/ heavy HAP1-ΔOSCP cells was re-calculated (median of peptide ratios) using all the available peptide values (n=174; $\log_2$ protein ratio -4.42) rather than the MaxQuant value ($\log_2$ protein ratio -4.37) obtained using four MULTIMSMS peptide ratios assigned for peptide pairs with a control sequence identified by MS-MS and an isotopic cluster for the ΔOSCP partner. Total RNA was purified from HAP1-Δb cells with a PureLink RNA mini kit (ThermoFisher). Any remaining traces of genomic DNA were removed by digestion with RNase-free DNase I. At the end of the digestion, DNase I was inhibited with the DNase inactivation reagent (ThermoFisher). cDNA was prepared from the RNA by reverse transcription using the RT enzyme mix and buffer from a TaqMan Gene Expression Cells-to-CT Kit (ThermoFisher). The regions of *ATP5F1* from the 40th nucleotide upstream of the ATG start codon to the junction between exons V and VI, and exons VI and VII of *ATP5F1*, respectively (Fig. S1A), were amplified with a KOD Hot Start DNA polymerase kit (Novagen) with forward primer 5' CACAGGGACGCTAAGATTG 3' paired with the reverse primer Rev1, 5' GTTTTTGCTCATTGAGTTTATC 3', or Rev2, 5' CTCCTTTTCCTGCTGTGTG 3'. The amplified fragments were purified with a gel purification kit (Qiagen) and sequenced with reverse primer Rev1 or Rev2 by Source BioScience.

Opening of the PTP. Four independent assays of PTP opening were used. In intact human cells, PTP opening was induced by thapsigargin (7), or ferutinin (8), and, in cells where the

plasma membrane had been permeabilized with digitonin, by examination of the capacity of the mitochondria to retain Ca^{2+} introduced exogenously (9) or by monitoring PTP induced swelling of mitochondria (10). The assays with thapsigargin and ferutinin, and the calcium retention assay were performed as before (3), except that, in the buffer employed in the calcium retention assay, any initial background signal was removed by incorporation of EGTA (3 μM), and changes in exogenous calcium levels were measured with 0.4 μM calcium green-5N. Pore opening was monitored also by following absorbance changes associated with the swelling of mitochondria induced by the addition of Ca^{2+} in the absence and presence of cyclosporin A. Digitonin permeabilized cells (30 x 10^6/ml) were suspended at 30°C in a buffer containing 10 mM Tris-MOPS, pH 7.4, 125 mM KCl, 1 mM KH_2PO_4, 5 mM glutamate, 2.5 mM malate and 10 μM EGTA-Tris, and stirred at 500 rpm. Calcium chloride (200 μM) was added, and the decrease in UV absorbance at 540 nm was followed. The effect of cyclosporin A on calcium induced swelling of mitochondria, was studied by adding the inhibitor (1 μM) to the permeabilised cells first, and, after 5 min, the 200 μM calcium chloride.

Table S1. Target Sites for gRNA Molecules Employed in the Disruption of Human *ATP5F1* and *ATP5O*.

gRNA	Target site
ATP5F1-1	GGGACGCTAAGATTGCTACC
ATP5F1-2	CCGCCGCCACAGCGGGTAAG
ATP5O-1	GAGAACCTAGCGGTTACGCC*
ATP5O-2	CCAGGGTGCGATGCTTCGGC

*reverse complementary sequence used as the gRNA

Table S2. Primers Employed in the Amplification by PCR of the Gene Regions Targeted by gRNAs in *ATP5F1* and *ATP5O*.

Primer	Sequence
ATP5F1-forward	CATCTTGGTCCTGCCCTGAC
ATP5F1-reverse	GCTGCAGATAGACAAGGCGA
ATP5O-forward	TACAACTCCCAGCCCGAGG
ATP5O-reverse	ACGCCAAGGTTACGGCA

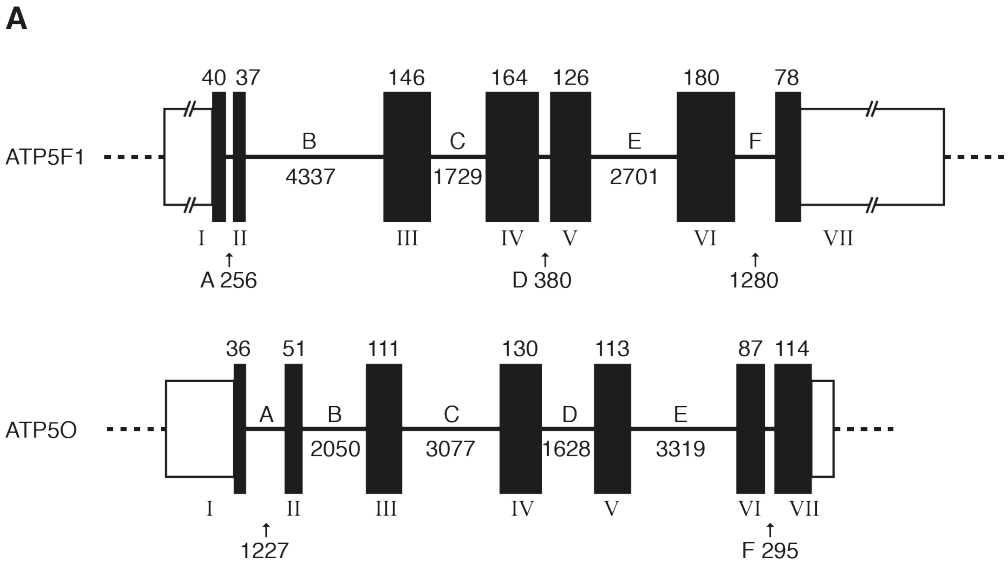

B

```
WT      GTCACAGGGACGCTAAGATTGCTACCTGGACTTTCGTTGACCATGCTGTCCCGGGTGGTA
Δb      GTCACAGGGACGCTAAGATTGC------------------------------------

WT      CTTTCCGCCGCCGCCACAGCGGGTAAGGGGTATAGACCCTGCTCTGGA
Δb      ------------------------AAGGGGTATAGACCCTGCTCTGGA


WT      CTTCCCAGAGAACCTAGCGGTTACGCCAACGCGCGCGTGCGCCCTTGCGCGTTTCTCTCT
ΔOSCP   CTTCCCAGA-------------------------------------------------

WT      TCCCACTCGGGTTTGACCTACAGCCGCCCGGGAGAAGATGGCTGCCCCAGCAGTGTCCGG
ΔOSCP   ---------------------------------------------------------

WT      GCTCTCCCGGCAGGTGAGAGAAAGGTGGTCCTGAGAGCCAGTGGGAGGATCCCTCCTGGG
ΔOSCP   ---------------------------------------------------------

WT      ATGACCGGTACCAAACCTCGAGCACCAGGGTGCGATGCTTCGGCTGGGGAAGTC
ΔOSCP   ------------------------------------------CCTGGGGAAGTC
```

Fig. S1. Structures and disruption of *ATP5F1* and *ATP5O*. (*A*) Structures of the genes. Black and unfilled boxes represent, respectively, protein coding exons and non-coding 5'-upstream or 3'-downstream sequences within the first and last exons. Introns are depicted as continuous lines. Sizes of the exons and introns are given in base pairs. (*B*) Deletion of DNA sequences in HAP1-WT cells to produce HAP1-Δb or HAP1-ΔOSCP clonal cells. Carets indicate the PAM (protospacer adjacent motif) sequences for each guide RNA, and solid lines the guide RNA target sequences. For each gene, the upper WT sequences show part of exon I and intron A

(grey box), with the arrow indicating the start codon in exon I. Dashed lines denote the deleted regions in the HAP1-Δb and HAP1-ΔOSCP cells. Both deletions remove the start codon and exon I-intron A boundaries, thereby effectively disrupting transcription and translation of the genes.

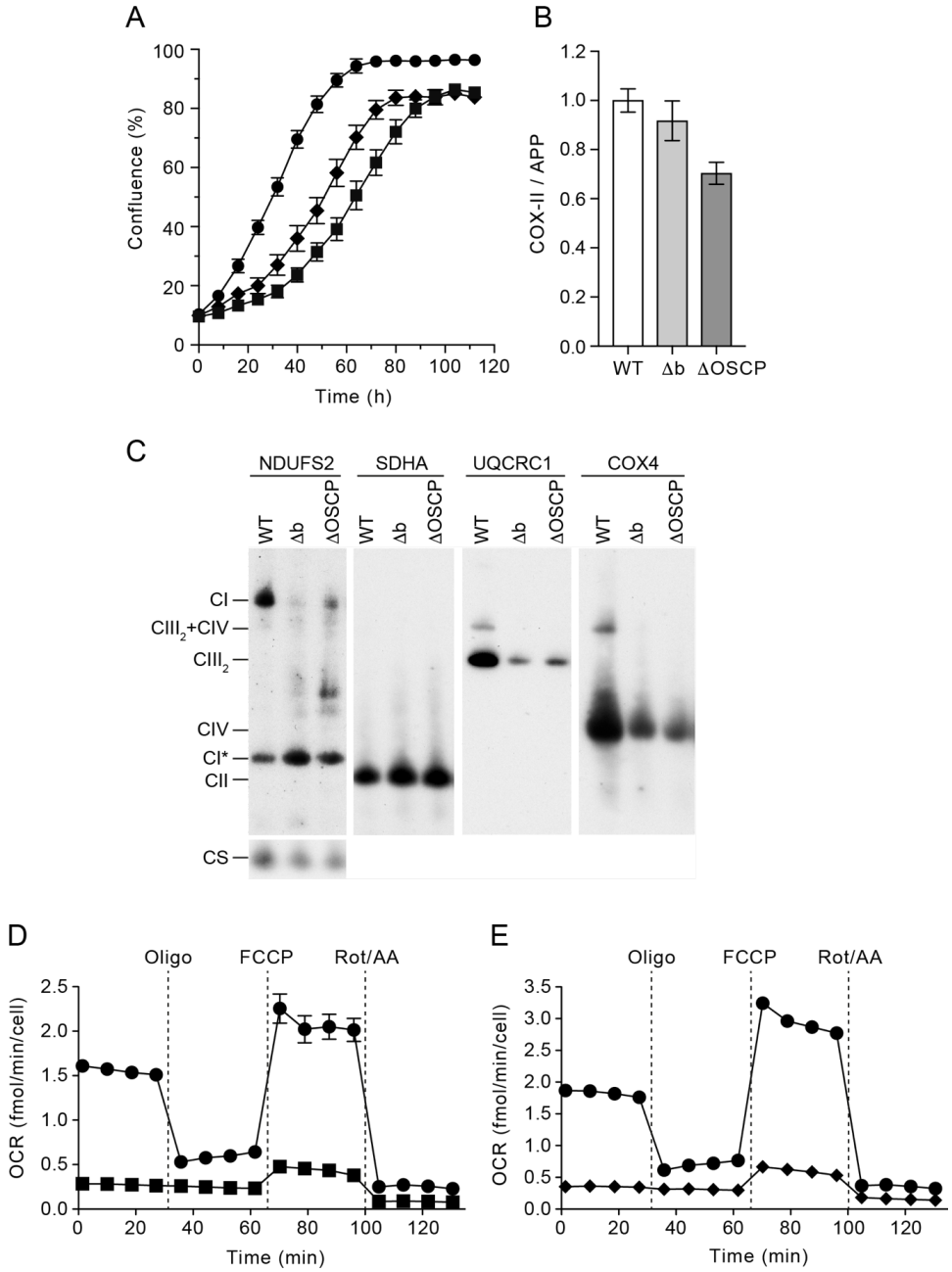

Fig. S2. Characteristics of HAP1-Δb cells and HAP1-ΔOSCP cells. (*A*) Growth rates of HAP1-WT (●), HAP1-Δb (■) and HAP1-ΔOSCP (◆) cells. About 100,000 cells were seeded into each well of a 6-well plate, and their confluence was monitored over 120 h. Data points are the mean values ±SD (n=4). (*B*) Relative copy number of mtDNA in HAP1 cells. Regions of the genes for cytochrome oxidase subunit II (COX-II) and the amyloid precursor protein (APP) were amplified from HAP1-WT, HAP1-Δb and HAP1-ΔOSCP cells, and quantitated as indices of mitochondrial and nuclear DNA, respectively. Mean values ± SDs (n=6) are given. (*C*)

Assembly of complexes I, II, III and IV in HAP1 cells. Mitoplast samples were prepared from HAP1-WT cells and HAP1-Δb and HAP1-ΔOSCP cells, extracted with DDM (3 g/g mitoplast protein), and the extracts were fractionated by BN-PAGE. Complexes were detected by western blotting with antibodies against complex I (NDUFS2), complex II (SDHA), complex III (UQCRC1) and complex IV (COX4). Citrate synthase (CS) provided a loading control. CI, complex I; $CIII_2$, complex III dimer; CIV, complex IV; $CIII_2$+CIV, complex III dimer plus complex IV; CI*, complex I sub-complex. (*D* and *E*), cellular oxygen consumption rates (OCR) of HAP1-WT (●), HAP1-Δb (■) and HAP1-ΔOSCP (◆) cells, before and after sequential addition of oligomycin (Oligo), carbonyl cyanide-4-(trifluoromethoxy)-phenylhydrazone (FCCP), and a mixture of rotenone and antimycin A (Rot/AA). Data represent the mean ±SEM (n=6-10 wells).

Table S3. Number of Calcium Pulses Recorded in Permeabilized HAP1-WT Cells.

The values in the first row refer to Fig. 4A and B. Rows 2-8 correspond to replicate experiments.

No CsA	With CsA	Ratio
5	12	2.40
6	16	2.67
3	8	2.67
11	26	2.36
6	22	3.67
7	20	2.86
7	15	2.14
4	9	2.25
Av. 6.1	Av. 16.0	Av. 2.63
SD. 2.4	SD. 6.3	SD. 0.48

Table S4. Number of Calcium Pulses Recorded in Permeabilized HAP1-Δb Cells.

The values in the first row refer to Fig. 4C and D. Rows 2-4 correspond to replicate experiments.

No CsA	With CsA	Ratio
4	12	3.00
5	13	2.60
3	7	2.33
3	6	2.00
Av. 3.8	Av. 9.5	Av. 2.48
SD. 1.0	SD. 3.5	SD. 0.42

Table S5. Number of Calcium Pulses Recorded in Permeabilized HAP1-ΔOSCP Cells.

The values in the first row refer to Fig. 4E and F. Rows 2-6 correspond to replicate experiments.

No CsA	With CsA	Ratio
6	16	2.67
7	18	2.57
4	7	1.75
3	7	2.33
3	6	2.00
3	6	2.00
Av. 4.3	Av. 10.0	Av. 2.22
SD. 1.8	SD. 5.5	SD. 0.36

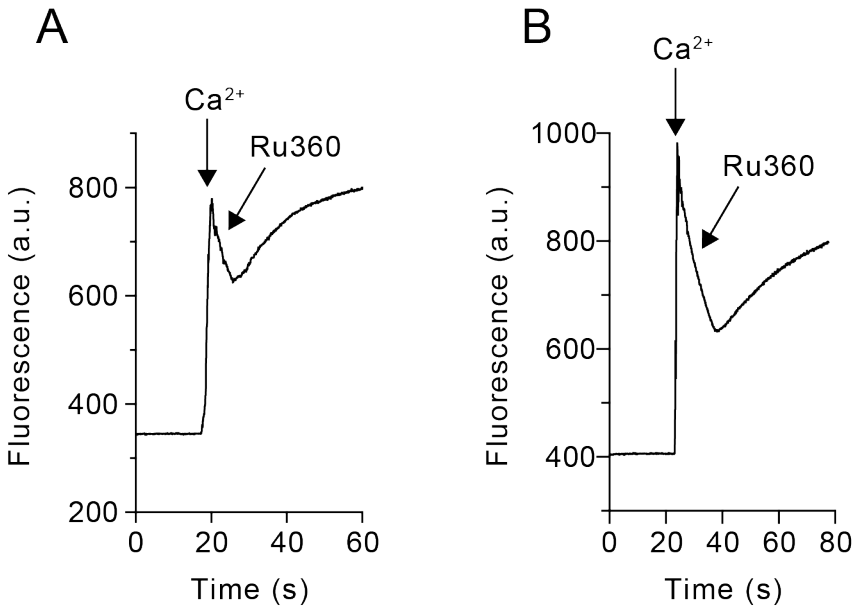

Fig. S3. Calcium uptake by HAP1 cells in the presence of Ru360, an inhibitor of the mitochondrial calcium uniporter. Digitonin permeabilized HAP1-WT cells (*A*) and HAP1-Δb cells (*B*) at 20 x 10^6 cells/ml in a KCl solution containing glutamate and malate (3), were subjected to a single pulse of 10 μM $CaCl_2$, followed by the addition of Ru360 (0.5 μM). Extramitochondrial calcium was measured with calcium green-5N fluorescence which demonstrated that Ru360 reversed the mitochondrial calcium uptake signal.

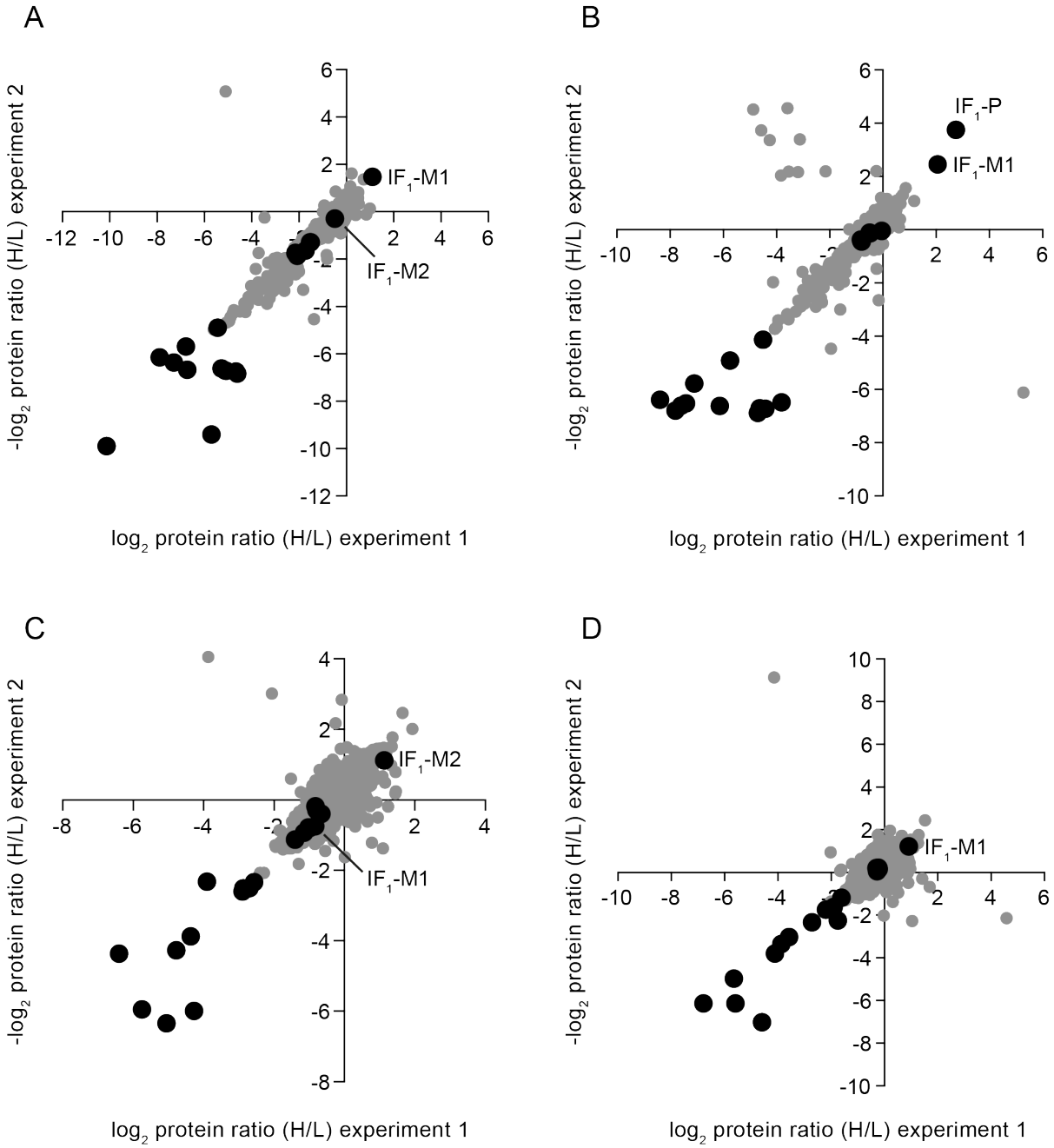

Fig. S4. Effects on protein relative abundance of the individual deletion of the b-subunit or OSCP of human ATP synthase in HAP1 cells. (*A*) and (*B*) the relative abundances of proteins in HAP1-Δb and HAP1-ΔOSCP immunopurified ATP synthase, respectively, and (*C*) and (*D*) mitoplast samples from HAP1-Δb and HAP1-ΔOSCP cells, respectively. Samples were prepared from a 1:1 mixture of HAP1-Δb or HAP1-ΔOSCP cells with HAP1-WT cells that were differentially SILAC-labelled, and the experiments were performed twice, using reciprocal SILAC labelling orientations. The data points represent levels of all proteins where

ratios were determined in both of the experimental labelling orientations. ●, ATP synthase subunits and the precursor (P), or the M1 and M2 mature forms of IF_1; ●, all other identified proteins. Protein ratios are listed in Datasets S1 to S4.

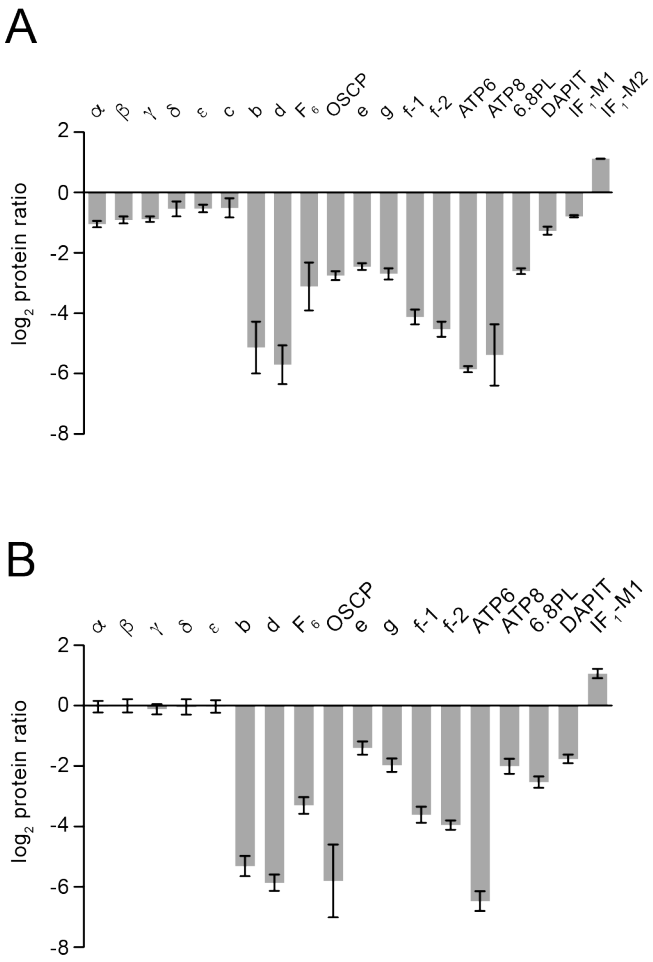

Fig. S5. Effects of the separate deletion of the b-subunit and OSCP in HAP1 cells on the levels of ATP synthase subunits in mitoplasts. (*A*) and (*B*) Relative abundance of subunits of ATP synthase and of two forms of the ATPase inhibitor protein (3). Digitonin solublilized mitoplast samples were prepared from a 1:1 mixture of SILAC-labelled HAP1-WT cells and HAP1-Δb cells (*A*), or HAP1-WT cells and HAP1-ΔOSCP cells (*B*). Proteins were separated by SDS-PAGE, stained with Coomassie blue, and gel tracks cut into equal sections. Tryptic peptides obtained from in-gel digests were analyzed by quantitative mass spectrometry. The experiment was performed twice with reciprocal protein labelling. The bars represent median values of both relative abundance ratios determined for proteins identified in the complementary SILAC labelling experiments. Error bars show the range of the two values. The relative abundance of

the c subunit in HAP1-ΔOSCP samples was not determined. The histograms are derived from the data in Fig S4 and Datasets S3 and S4.

Fig. S6. Alternative splice site between exon I and intron A formed in *ATP5F1* in HAP1-Δb cells. (*A*), The upper sequence is part of exon I and intron A (grey box) in HAP1-WT cells, with the horizontal arrow indicating the start codon in exon I. The vertical arrows show a splice site between exon I and intron A in HAP1-WT cells (upper sequence) and alternative splice site in HAP1-Δb cells (lower sequence). Dashed lines denote the deleted region in *ATP5F1* in HAP1-Δb cells. (*B*) The protein encoded from the alternative transcript in HAP1-Δb cells. The upper sequence shows the WT protein with the horizontal arrow indicating the start of the mature protein, and lower sequence the truncated protein produced in HAP1-Δb cells. Peptides assigned to the truncated protein cover the regions within the grey boxes.

Table S6. Sources of antibodies

Protein	Source	Antibody
ATP synthase β	Santa Cruz Biotechnology	sc-33618
ATP synthase F_6	Proteintech	14114-1-AP
ATP synthase b	Santa Cruz Biotechnology	sc-514419
ATP synthase d	In-house	Rabbit antibody against recombinant bovine protein
ATP synthase g	In-house	Rabbit antibody against recombinant bovine protein
ATP synthase OSCP	In-house	Rabbit antibody against recombinant bovine protein
Citrate synthase	Proteintech	16131-1-AP
Complex I NDUFS2 subunit	Abcam	ab96160
Complex II SDHA subunit	Proteintech	14865-1-AP
Complex III UQCRC1 subunit	Sigma	HPA002815
Complex IV COX4I1 subunit	Proteintech	11242-1-AP

References

1. Ran FA *et al.* (2013) Genome engineering using the CRISPR-Cas9 system. *Nat Protoc* 8(11):2281–2308.
2. Klement P, Nijtmans LG, Van den Bogert C, Houstěk J (1995) Analysis of oxidative phosphorylation complexes in cultured human fibroblasts and amniocytes by blue-native-electrophoresis using mitoplasts isolated with the help of digitonin. *Anal Biochem* 231(1):218–224.
3. He J *et al.* (2017) Persistence of the mitochondrial permeability transition in the absence of subunit c of human ATP synthase. *Proc Natl Acad Sci U S A* 114(13):3409–3414.
4. Wilm M *et al.* (1996) Femtomole sequencing of proteins from polyacrylamide gels by nano-electrospray mass spectrometry. *Nature* 379(6564):466–469.
5. Ong SE *et al.* (2002) Stable isotope labeling by amino acids in cell culture, SILAC, as a simple and accurate approach to expression proteomics. *Mol Cell Proteomics* 1(5):376–386.
6. Cox J, Mann M (2008) MaxQuant enables high peptide identification rates, individualized p.p.b.-range mass accuracies and proteome-wide protein quantification. *Nat Biotechnol* 26(12):1367–1372.
7. Korge P, Weiss JN (1999) Thapsigargin directly induces the mitochondrial permeability transition. *Eur J Biochem* 265(1):273–280.
8. Abramov AY, Duchen MR (2003) Actions of ionomycin, 4-BrA23187 and a novel electrogenic Ca^{2+} ionophore on mitochondria in intact cells. *Cell Calcium* 33(2):101–112.
9. Murphy AN, Bredesen DE, Cortopassi G, Wang E, Fiskum G (1996) Bcl-2 potentiates the maximal calcium uptake capacity of neural cell mitochondria. *Proc Natl Acad Sci U S A* 93(18):9893–9898.

10. Clarke SJ, McStay GP, Halestrap AP (2002) Sanglifehrin A acts as a potent inhibitor of the mitochondrial permeability transition and reperfusion injury of the heart by binding to cyclophilin-D at a different site from cyclosporin A. *J Biol Chem* 277(38):34793–34799.